Radiative Effects of Elevated Pollutant Layers

A. VENKATRAM[1]

Air Quality and Inter-Environmental Research Branch, Atmospheric Environment Service, Downsview, Ontario, Canada M3H 5T4

R. VISKANTA

School of Mechanical Engineering, Purdue University, West Lafayette, Ind. 47907

(Manuscript received 16 June 1977, in revised form 24 September 1977)

ABSTRACT

A one-dimensional transport model was developed to study the effects of radiative participation of elevated pollutant layers. Special features of the model include a turbulent kinetic energy model and a two-stream solar radiation model. Pollutants were assumed to consist of aerosols and pollutant gases. Aerosols were allowed to scatter and absorb energy in the solar spectrum while pollutant gases were assumed to interact only with thermal radiation.

The results of the simulations conducted with the model showed that elevated layers of pollutants could control mixed-layer expansion by modifying the stability of the capping stable layer. Cooling associated with gaseous pollutants generally helped the growth of the mixed layer, while solar heating induced by pollutants hindered mixed-layer growth by creating sharp inversions.

By affecting mixed-layer growth, radiative participation by pollutants also modified pollutant dispersal from the elevated pollutant layer. These results have important implications from the point of air pollution meteorology (especially fumigation) in which it is generally assumed that pollutants are passive.

1. Introduction

Pollutant-induced radiative heating or cooling is clearly of most significance in regions of the PBL where the competing transport mechanism, turbulence, is inhibited. Thus it would seem that elevated layers of radiatively active pollutants could play the major role in modifying the structure of the relatively nonturbulent upper regions of the PBL. This modification is important in view of the fact that the expansion of the convective boundary layer depends on the stability of the capping inversion (Tennekes, 1974).

Elevated pollutant layers can occur in several ways. Pollutants which are vertically dispersed during the growth of the daytime boundary layer can form elevated layers when the mixed layer collapses after sunset. They can also result from the emission of pollutants from tall smoke stacks which can be as high as 380 m (Lusis and Wiebe, 1976). This paper addresses itself to the possible radiative effects these elevated pollutant layers can induce. Specifically, we will investigate pollutant induced effects on mixed-layer growth and dispersion inside the mixed layer. Previous studies on the possible radiative interaction of pollutants have given only peripheral attention to the problem addressed to in this paper. Bergstrom and Viskanta (1973) and Zdunkowski *et al.* (1976) have pointed out the importance of radiative transport in the dynamics of the PBL but have not considered the effects associated with elevated pollutant layers. Atwater (1970) raised the possibility of pollutant layers leading to the formation of elevated inversions; however, he did not investigate the role of these inversions in modifying the growth of the mixed layer.

An important difference between our study and those of others lies in the modeling of turbulent transport. In this investigation we have used a modified version of the turbulent kinetic energy model which in the opinion of several investigators (Taylor, 1974; Lykosov, 1972) represents a compromise between simplistic Richardson number correlation models (used in other studies similar to ours) and numerically cumbersome higher order models (Wyngaard *et al.*, 1974; Donaldson, 1973). The model will be discussed in more detail in a later section.

The primary emphasis of this paper is on the role of elevated pollutant layers in modifying the growth dynamics of the mixed layer. In incorporating a realistic turbulence model we believe we have made an improvement over previous efforts at modeling radiative effects of pollutants.

[1] Present affiliation: Air Quality and Meteorology Section, Air Resources Branch, Ontario Ministry of the Environment, Toronto, Ontario, Canada M5S 1Z8.

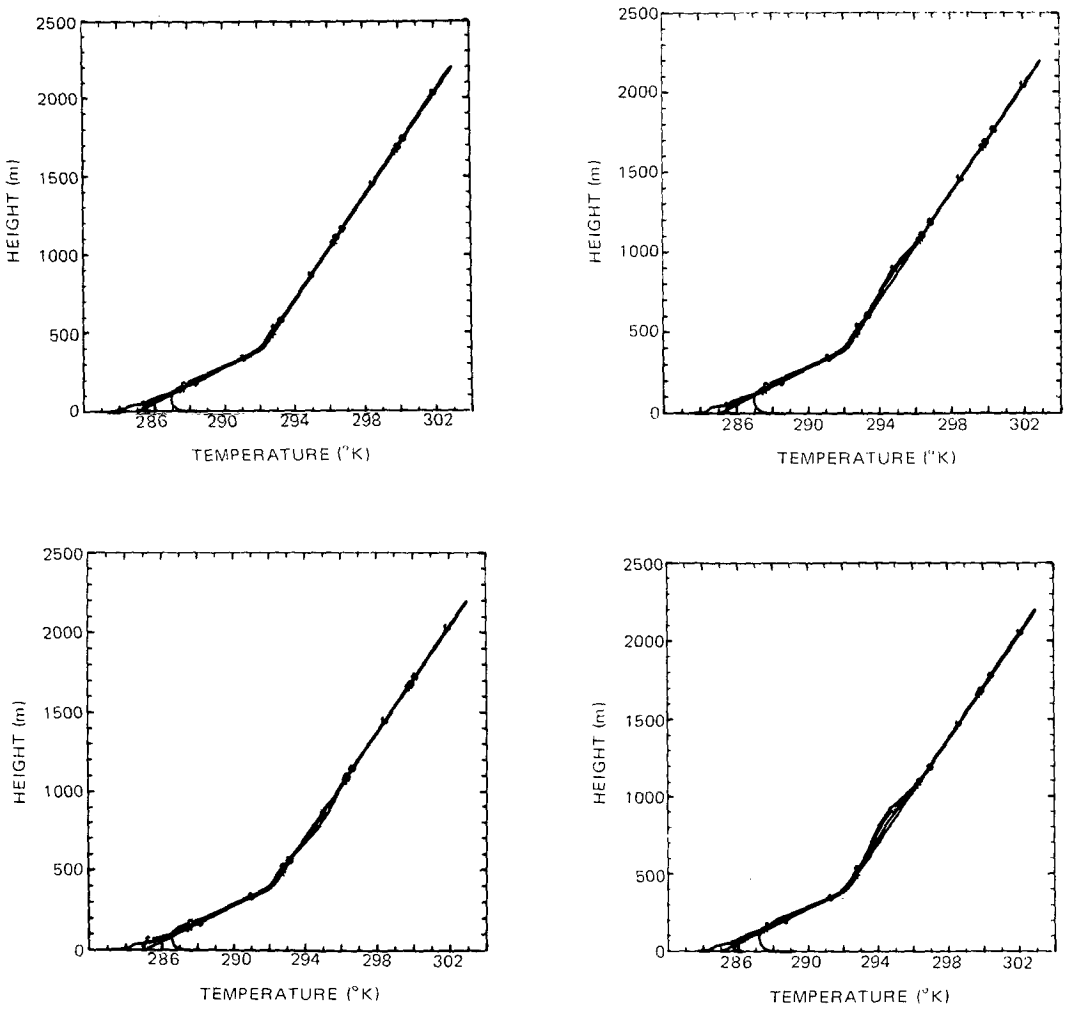

FIG. 1. Potential temperature profiles for 0500–0800 local time, O'Neill, Nebr. Top left is simulation NP, top right simulation P, bottom left simulation SP and bottom right simulation TP. Elevated pollutant layer at 300 m.

2. Analysis

a. *Physical model*

The physical model is assumed to consist of four layers: 1) the "free" atmosphere where the atmospheric variables are determined by the large-scale flow [as the simulation time scale of the model is relatively small (48 h), the free atmospheric variables can be assumed to be unaffected by the flow in the boundary layer]; 2) the "polluted" atmosphere in which the atmospheric variables such as velocities, temperature and pollutant concentrations are functions of space and time, and change in response to varying boundary conditions primarily at the lower boundary (earth–air interface) and at the upper boundary (free atmosphere); 3) the soil layer in which the temperature is a function of depth and time only; and 4) the lithosphere in which the temperature below the soil layer is constant over the time scale of simulation.

As the primary emphasis of this study is on a specific effect induced by pollutants we have chosen to model a one-dimensional PBL. We can provide additional justification for this assumption by noting that pollutants are most likely to have the greatest effect on thermal structure through radiative participation when advection is small, i.e., stagnating high pressure centers with light winds.

b. *Basic equations*

The model equations are the same set used by previous investigators (Estoque, 1963; Sasamori, 1970). They are as follows (see Appendix for list of symbols):

Boundary Layer

$$x\text{-momentum:}\quad \frac{\partial u}{\partial t}=f(v-v_g)+\frac{\partial}{\partial z}\left(K_M\frac{\partial u}{\partial z}\right) \tag{1}$$

$$y\text{-momentum:}\quad \frac{\partial v}{\partial t}=-f(u-u_g)+\frac{\partial}{\partial z}\left(K_M\frac{\partial v}{\partial z}\right) \tag{2}$$

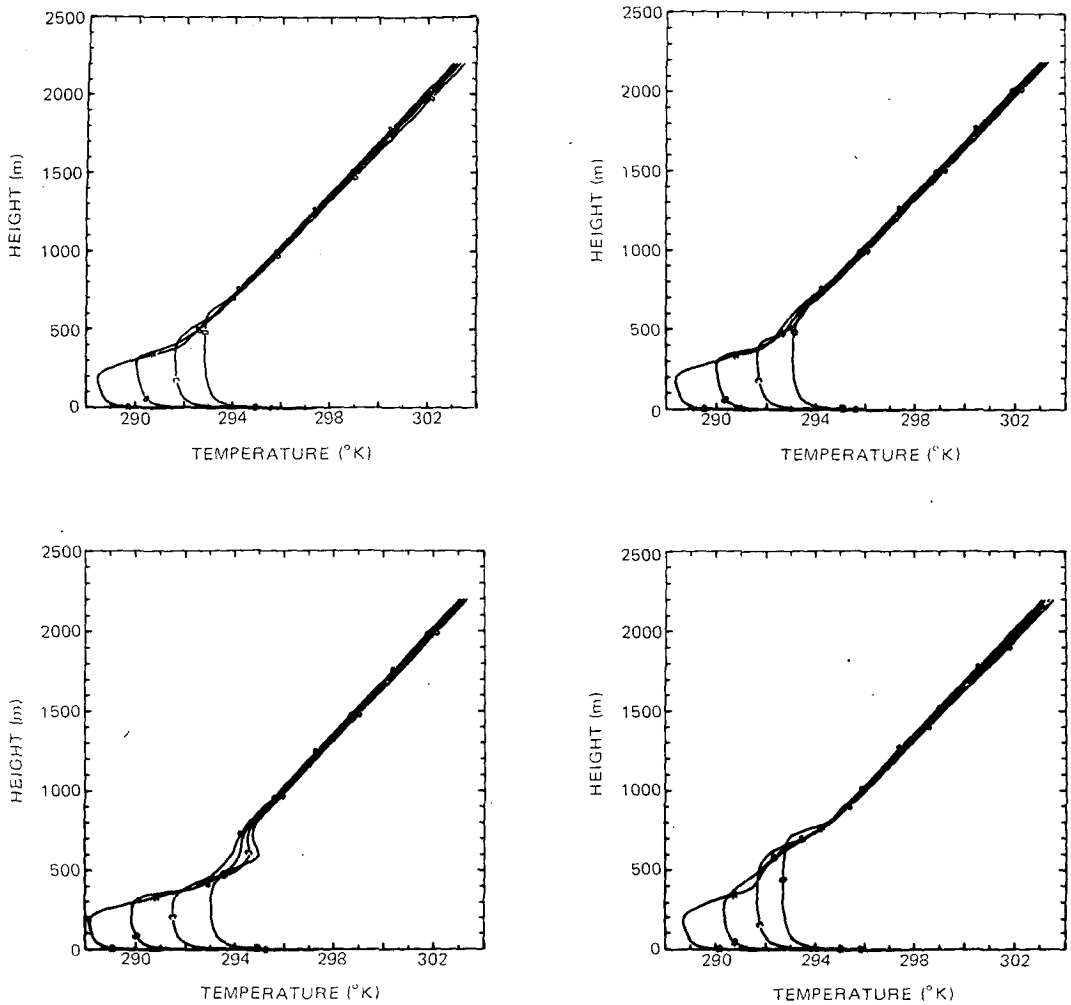

FIG. 2. As in Fig. 1 except for 0900–1200.

$$z\text{-momentum:}\quad \frac{\partial p}{\partial z}=-\rho g \tag{3}$$

$$\text{Energy:}\quad \frac{\partial \theta}{\partial t}=\frac{\partial}{\partial z}\left[K_H\left(\frac{\partial \theta}{\partial z}-\gamma_c\right)\right]-\left(\frac{p_0}{p}\right)^{R/c_p}\frac{\partial F}{\partial z} \tag{4}$$

$$\text{Species:}\quad \frac{\partial C_n}{\partial t}=\frac{\partial}{\partial z}\left(K_C\frac{\partial C_n}{\partial z}\right)+\dot{S}_{C_n},\quad n=1,2 \tag{5}$$

Soil Layer

$$\text{Energy:}\quad \frac{\partial T_s}{\partial t}=\alpha_s\frac{\partial^2 T_s}{\partial z^2}. \tag{6}$$

In Eq. (4) γ_c is a small positive quantity to account for the counter-gradient heat flux observed (Telford and Warner, 1964) in the convective boundary layer. Deardorff (1967) recommends a value of 0.7×10^{-3} °C m^{-1} for γ_c.

The boundary conditions are specified at the top ($z=2000$ m) and bottom ($z=z_0$) of the atmospheric layer under consideration. It is necessary to distinguish between the top of the boundary layer and the top of the atmospheric layer. The boundary layer is the region of the atmospheric layer which is turbulent. Thus, in this study, the height of the boundary layer is given by the lowest grid level at which the turbulent kinetic energy goes to zero. This definition is the same as that used by Lykosov (1972).

At the air–soil interface the boundary conditions are

$$u=v=0,\quad \theta=\theta_0(t),\quad C_n=C_{n0}(t). \tag{7a}$$

The surface temperature $\theta_0(t)$ is calculated from an energy balance (Estoque, 1963):

$$R_n-H_T-H_L-H_S-\sigma\theta_0^4=0, \tag{7b}$$

where R_n is the net (solar plus thermal) radiative flux at the surface, H_T the turbulent heat flux away from the surface and H_L the latent heat flux. Details of the

solution of (7b) can be found elsewhere (Venkatram and Viskanta, 1976).

The pollutant concentration at the surface $C_{n0}(t)$ is given by specifying the pollutant source strength as

$$M_{C_n} = -K_c \partial C_n / \partial z \quad \text{at } z=0. \tag{8}$$

The surface water vapor concentration is calculated by postulating that the ratio of the actual evaporation rate to the potential evaporation rate is a constant (Halstead *et al.*, 1957).

The boundary conditions at the top of the atmospheric layer ($z=H$) are specified by requiring the values of the atmospheric variables to remain constant.

At the bottom of the soil layer the temperature is taken to be a constant, i.e.,

$$T_s(z,t) = \text{constant at } z = -\Delta. \tag{9}$$

c. Turbulence model

The limitations of semi-empirical eddy diffusivity correlations have been clearly recognized and recent papers by Shir and Bornstein (1977) and Taylor (1974) discuss the need for improved models of turbulence. Richardson number correlations for eddy diffusivities are based on local equilibrium between production and dissipation of turbulence, an assumption which is reasonable only in the surface layer. Therefore their extension to the outer regions of the PBL cannot be justified on physical grounds. Furthermore, as the correlations are functions of local temperature and velocity gradients, they yield unrealistic results in regions in which gradients are small. This error is evident when we attempt to apply the correlations to the well-mixed daytime PBL. This limitation is all the more critical in our case as the focus of this study is the upper region of the PBL where gradients are typically small.

In this study we have used a turbulent energy model (Launder and Spalding, 1972). While avoiding the limitations of the Richardson number approach, we have incorporated an improved turbulence model. The additional computational effort involved is minimal as we add just one more equation to our original set. The equation expresses the conservation of turbulent

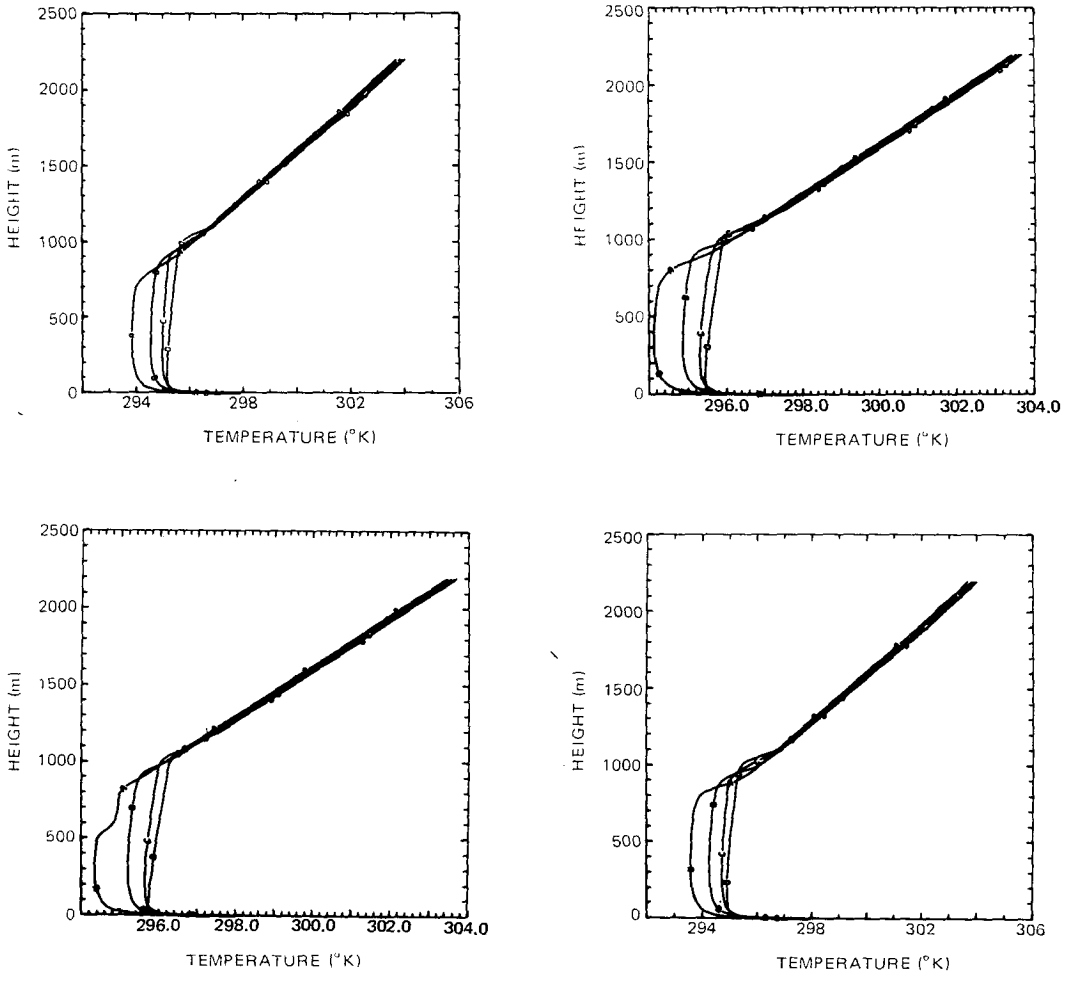

FIG. 3. As in Fig. 1 except for 1300–1600.

kinetic energy and includes transport terms in addition to the production and dissipation terms. The nonsteady nature of the equation allows for the realistic evolution of the turbulent kinetic energy. Also the transport terms ensure that the eddy diffusivity is not overly sensitive to local gradients of temperature and velocity.

The kinetic energy model has been developed and utilized by Launder and Spalding (1972) to model a wide variety of engineering flows. Peterson (1969) has applied the model to the problem of the modification of the planetary boundary layer by roughness changes under neutral conditions. Delage (1974) has applied the model to the nocturnal atmospheric boundary layer, and Lykosov (1972) has studied the diurnal variations of the boundary layer using a kinetic energy turbulence model. These and other studies indicate that the kinetic energy model is indeed an improvement over the Richardson number correlation approach.

The turbulent kinetic energy equation is presented below. The details of the derivation can be found in the book by Launder and Spalding (1972). With the usual closure assumptions (Launder and Spalding, 1972) the equation for the evolution of the turbulent kinetic energy k can be written as

$$\frac{\partial k}{\partial t}=\frac{\partial}{\partial z}\left(k^{\frac{1}{2}}l\frac{\partial k}{\partial z}\right)+K_M\left[\left(\frac{\partial u}{\partial z}\right)^2+\left(\frac{\partial v}{\partial z}\right)^2\right]-K_H\left[\left(\frac{\partial \theta}{\partial z}-\gamma_c\right)\right]\frac{g}{T}-C_D k^{\frac{3}{2}}/l, \quad (12)$$

where K_M and K_H are the eddy diffusivities for momentum and heat, respectively, and are given by

$$K_M=k^{\frac{1}{2}}l, \quad (13)$$

$$K_H=\alpha k^{\frac{1}{2}}l, \quad (14)$$

where $\alpha(=K_H/K_M)$ is taken to be the neutral value of 1.35 (Businger, 1972).

As the turbulent scales are very small near the earth's surface, a numerical solution of (12) would necessitate an impractically small time step to prevent the large

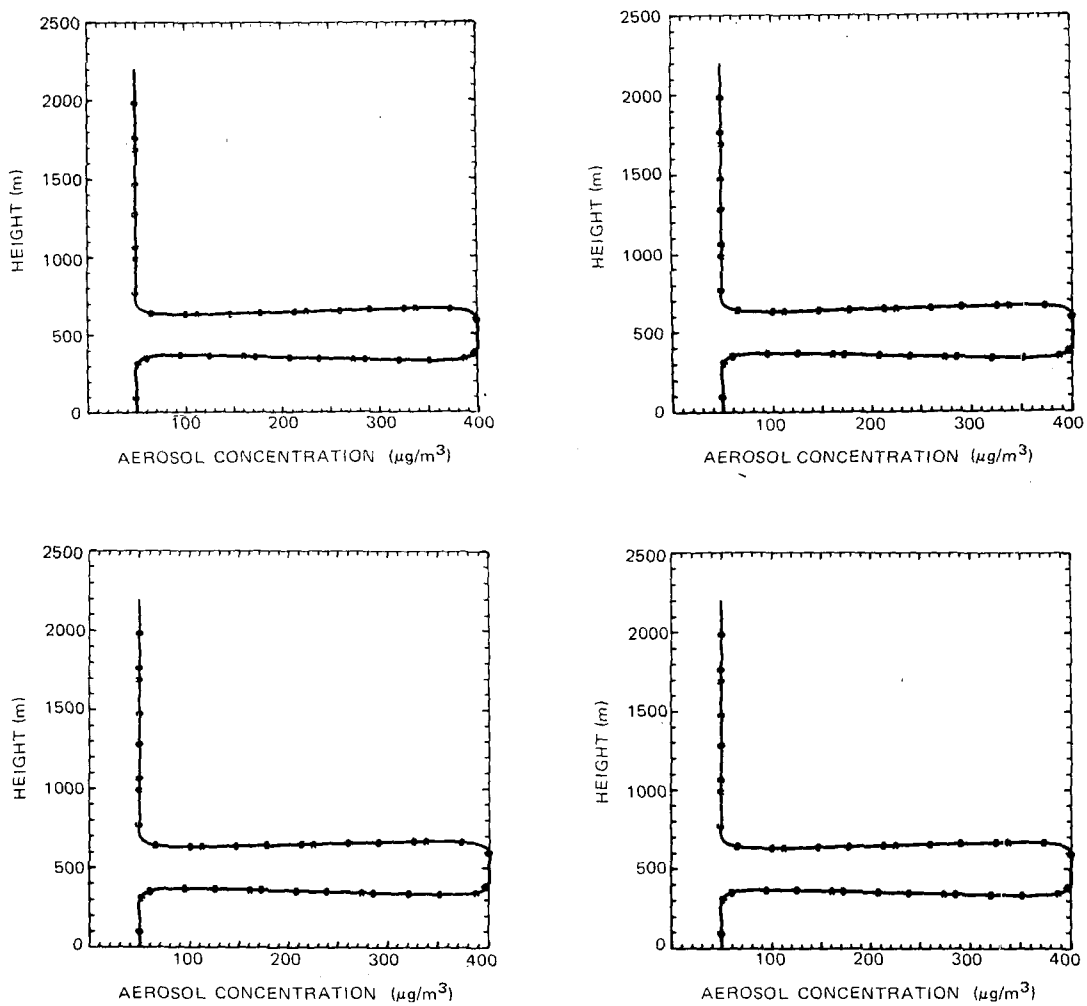

FIG. 4. Aerosol concentration profiles for 0500–0800. Otherwise as in Fig. 1.

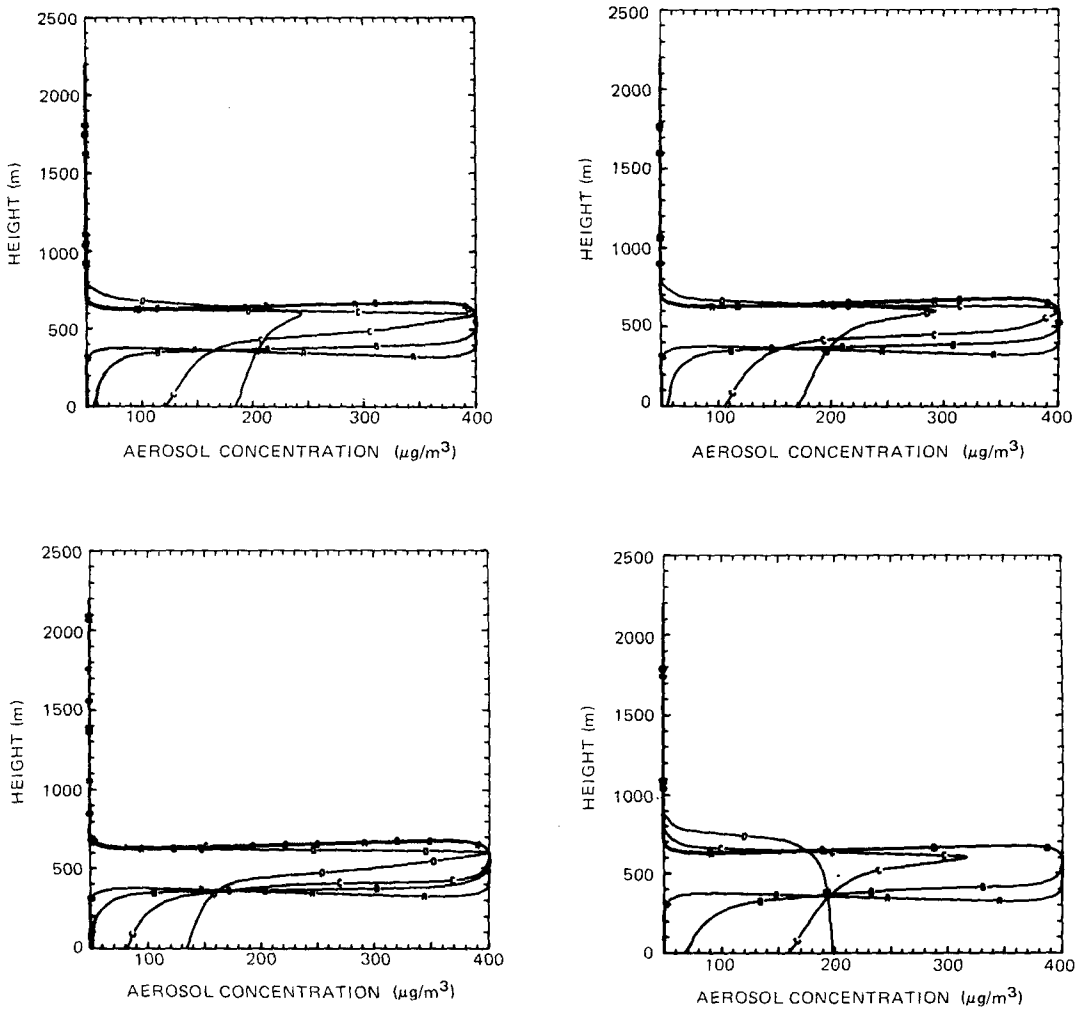

FIG. 5. As in Fig. 4 except for 0900–1200.

dissipation rates associated with the small length scales from driving the turbulent kinetic energy to physically unrealistic negative values. To avoid this problem we took advantage of the observed equilibrium between the production and dissipation of turbulent kinetic energy in the surface layer (Tennekes and Lumley, 1972). Using this observation the turbulent kinetic energy equation can be simplified to yield

$$k=\frac{l^2}{C_D}\left[\left(\frac{\partial u}{\partial z}\right)^2+\left(\frac{\partial v}{\partial z}\right)^2-\frac{\alpha g}{T}\left(\frac{\partial \theta}{\partial z}-\gamma_c\right)\right]. \quad (15)$$

The layer in which (15) is applicable is referred to as the equilibrium layer in this study. The equilibrium layer is similar to the constant flux layer used by boundary layer modelers (Estoque, 1963: Sasamori, 1970). Both the constant flux layer and the equilibrium layer are based on the principle of quasi-stationarity—negligible time lag between a physical change and the forcing causing the change. In fact, one would expect the thickness of the equilibrium layer to be of the same order of magnitude as that of the constant flux layer. Based on Estoque's (1963) value for the constant flux layer, the thickness of the equilibrium layer was chosen to be 50 m.

A solution of (12) requires a formulation for the mixing length l. We have chosen to specify the functional form of l rather than calculate it from a differential equation for a related quantity such as the dissipation rate as some investigators (Launder and Spalding, 1972; Wyngaard *et al.*, 1974) have done. A number of authors (Estoque, 1963; Yamada and Mellor, 1975) have utilized Blackadar's (1962) formulation for the mixing length. Although the formulation allows for a gradual leveling off of the mixing length in the upper part of the boundary layer, the relatively large mixing lengths tend to amplify small instabilities in the capping inversion. As the mixing length is associated with the dominant scale of turbulent motion, a model which predicts large mixing lengths in regions in which there is little or no turbulent activity is physically unrealistic. Clearly, a mixing length formulation should

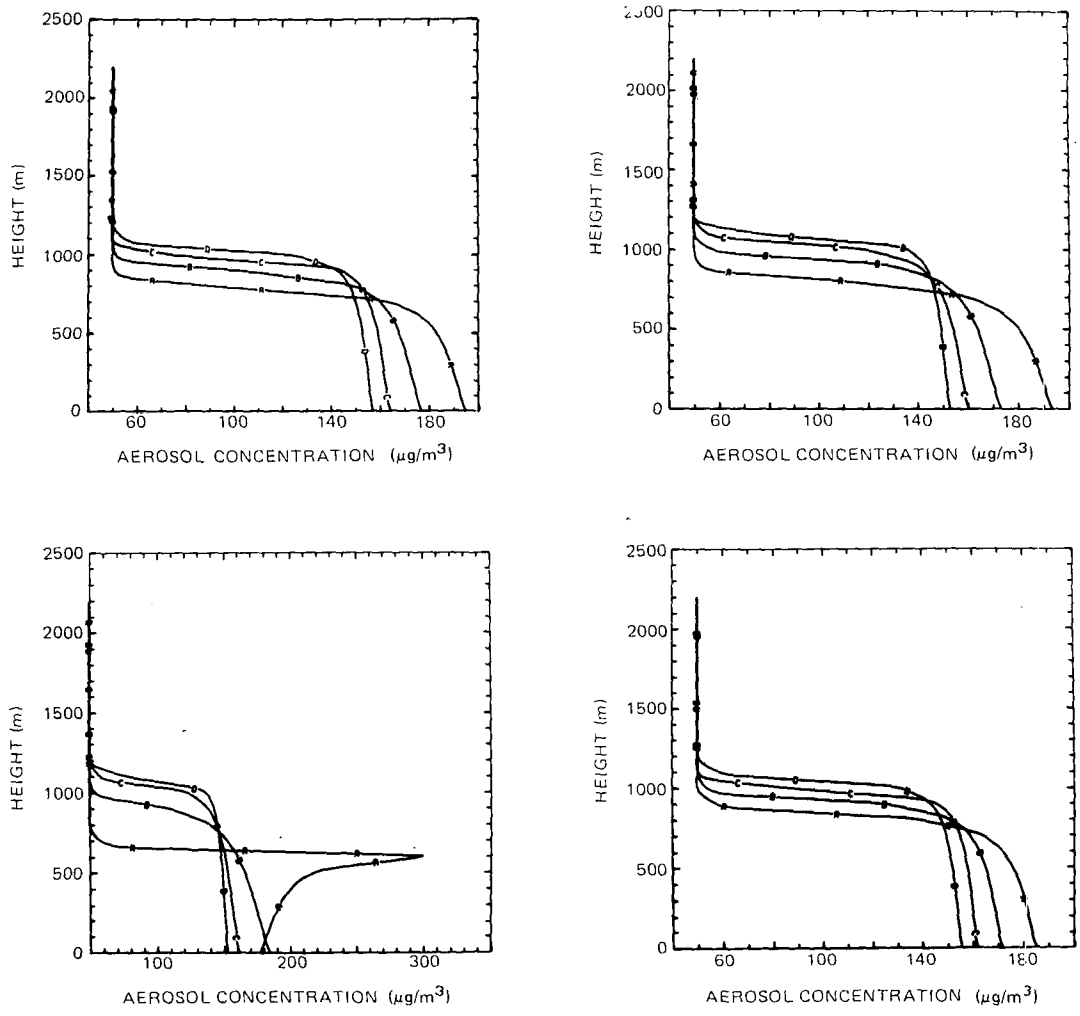

FIG. 6. As in Fig. 4 except for 1300–1600.

allow for a decrease of the mixing length in the upper part of the boundary layer. Recent experimental (Kalmykov *et al.*, 1975) as well as numerical studies (Deardorff, 1974) indicate that the mixing length does indeed decrease toward the edge of the boundary layer.

In order to allow for flexibility in the choice of the magnitudes of the mixing lengths at the middle and at the top of the boundary layer, we chose to represent l by a fourth-order polynomial, i.e.,

$$\bar{l}=a\eta+b\eta^2+c\eta^3+d\eta^4, \quad \eta=z/H_m. \tag{16}$$

The constants a, b, c and d in (16) are determined by the conditions

$$l=\begin{cases} C_D^{\frac{1}{2}}kz, & z=0 \quad (17a)\\ C_1H_m, & z=H_m/2 \quad (17b)\\ C_2H_m, & z=H_m. \quad (17c)\end{cases}$$

On the basis of Deardorff's (1974) study C_1 was chosen to be $0.8C_D$ and C_2 was rather arbitrarily chosen to be $0.1C_D$. Numerical experiments showed that the precise numerical value of C_1 was not important as long as it was small. It should be mentioned that polynomials have been used before (Sherstyuk, 1969) to describe mixing length behavior.

d. Radiation model

As is conventionally done, the spectrum of atmospheric radiation was divided into the solar region ($0.3\ \mu m \leqslant \lambda \leqslant 4\ \mu m$) and the thermal region ($4\ \mu m \leqslant \lambda \leqslant 100\ \mu m$). In the thermal spectrum multiple scattering was neglected. As the principle behind the emissivity approximation is now well enough established for most meteorological purposes, this study utilized empirical broad band emissivities to compute the thermal fluxes. For water vapor, the emissivity correlations derived from Kuhn's (1963) emission data were used. The carbon dioxide emissivity correlation utilized was the one proposed by Shekter (1950) and subsequently revised by Kondratyev (1969).

Clearly, gaseous pollutants have the greatest effect

when they interact with the relatively transparent atmospheric window extending from 8 to 12 μm. An examination of the absorption properties of a number of pollutant gases showed that ammonia was the best candidate for a representative "worst case" pollutant. Ammonia has its strongest band (at 300 K) centered at 10.5 μm and absorbs very strongly in the entire window region. Also, ammonia seems to be becoming an increasingly important air pollutant since it is associated with the presence of large populations (Ludwig *et al.*, 1969). This study utilized the wide band parameters derived by Tien (1973) from the France and Williams (1966) data on the infrared properties of ammonia.

An examination of the available methods to compute solar fluxes showed that the two-stream method met the requirement of computational convenience without introducing unacceptable idealizations such as neglect of multiple scattering. As the name implies, the method approximates the angular distribution of intensity by two intensities, one of which characterizes the radiation field in the forward direction and the other, in the backward direction. Also, the phase function is parameterized by introducing the forward and backward scattering factors which are the fractions of the radiative flux scattered in the forward and backward directions. The two-stream method has been used by Sagan and Pollack (1967) to study scattering in Venusian clouds and by Rasool and Schneider (1971) to study the effect of aerosols on global climate. More recently, Wang and Domoto (1974) have adapted the method to treat non-gray gaseous absorption with multiple scattering in the planetary atmosphere.

In the solar spectrum ($0.3\ \mu\text{m} \leqslant \lambda \leqslant 4\ \mu\text{m}$) emission of radiation can be neglected, and the radiative transfer equation for a plane-parallel atmosphere reduces to

$$\mu \frac{dI}{d\tau} = I + \frac{\omega}{2} \int_{-1}^{+1} p(\mu' \rightarrow \mu) I(\tau, \mu') d\mu', \qquad (18)$$

where I denotes the intensity, τ the optical depth, μ the cosine of the zenith angle, $p(\mu' \rightarrow \mu)$ the azimuthally averaged phase function and ω the single-scattering albedo. For reasons of convenience the dependence of the radiation parameters on the frequency ν and vertical coordinate z has been dropped.

The boundary conditions for (18) can be written as

$$I(0,\mu) = 2 \int_{0}^{+1} r_s(-\mu' \rightarrow \mu) I(0, -\mu') \mu' d\mu', \quad \mu > 0 \qquad (19)$$

$$I(\tau_0, \mu) = S\delta[\mu - (-\mu_0)] + I_d, \quad \mu < 0, \qquad (20)$$

where $r_s(-\mu' \rightarrow \mu)$ is the mean bidirectional reflectance of the earth's surface, τ_0 the optical thickness of the model layer, S the direct beam component (at zenith angle $\cos^{-1}\mu_0$) of the solar radiation at the top of the model layer and I_d the intensity of the diffuse component. Eq. (19) states that the intensity of the radiation traveling in the $+\mu$ direction (upward) at the earth's surface is the sum of the contributions from the beams of radiation reflected at the surface. Eq. (20)

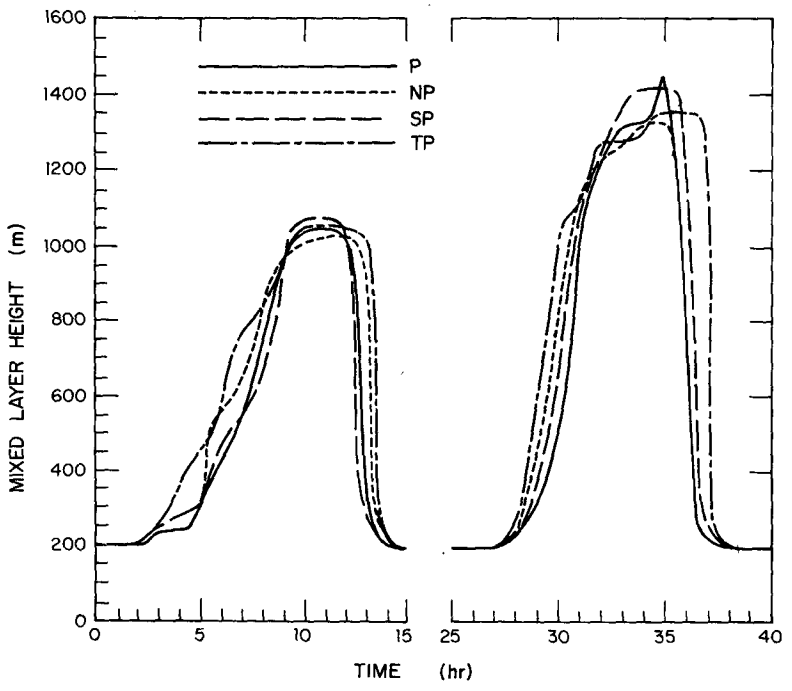

FIG. 7. Variation of mixed-layer height with time. Elevated pollutant layer at 300 m.

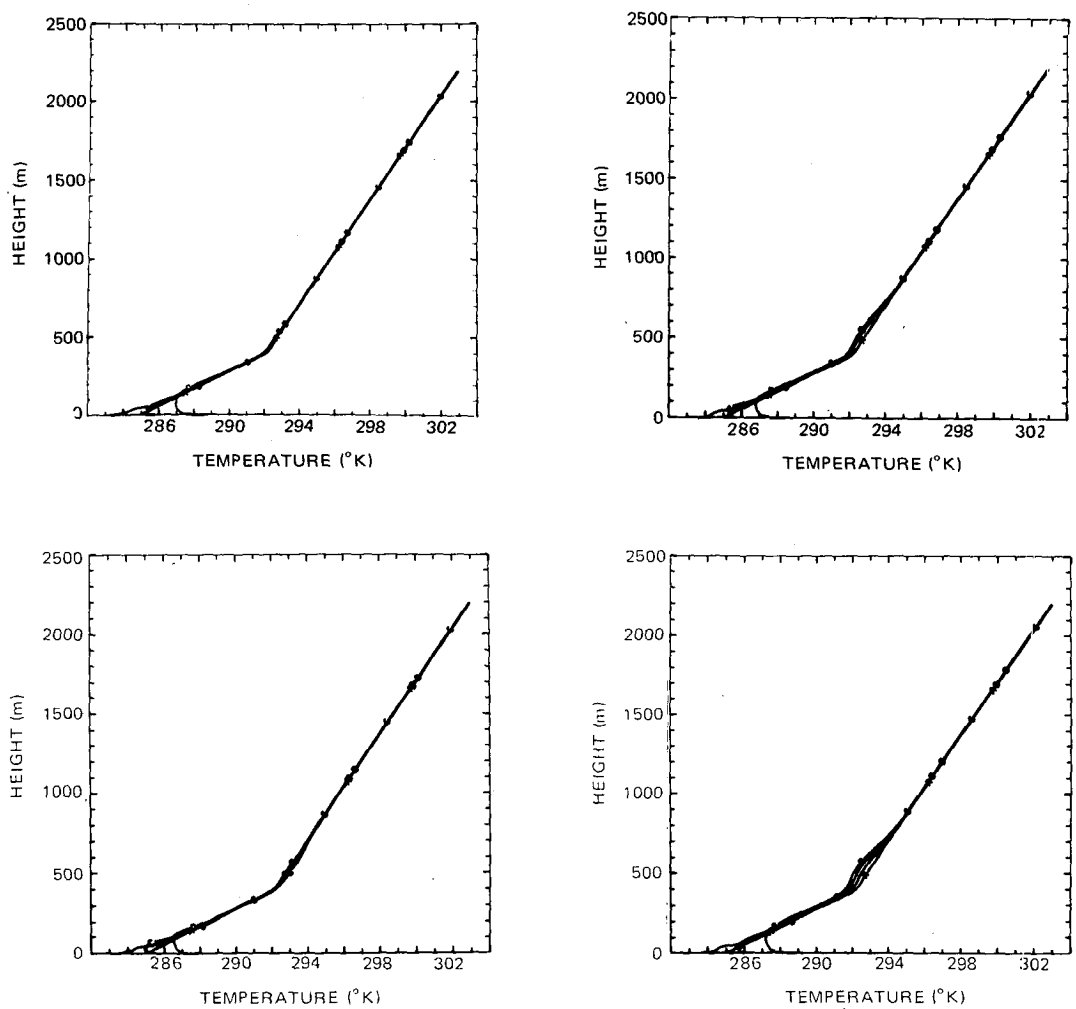

FIG. 8. Potential temperature profiles for 0500–0800 with elevated pollutant layer at 600 m.

specifies the direct (collimated) and diffuse solar fluxes at the top of the model layer.

The detailed derivation of the two-stream equations can be found elsewhere (Wang and Domoto, 1974) and need not be repeated here in detail. The general principle of the derivation can be explained as follows. The scattering phase function is expanded into a series of Legendre polynomials and the two-stream equations are obtained by substituting the expanded phase function into (24), multiplying the resulting equation by $d\mu$ and $\mu d\mu$, and integrating over μ from $+1$ to -1; the result may be written

$$\frac{1}{\sqrt{3}}\frac{dI^+}{d\tau}=(f\omega-1)I^+ + b\omega I^- + \tfrac{1}{2}\omega S[1-\sqrt{3}(1-2b)\mu_0] \times \exp[-(\tau_0-\tau)/\mu_0], \quad (21)$$

$$-\frac{1}{\sqrt{3}}\frac{dI^-}{d\tau}=(f\omega-1)I^- + b\omega I^+ + \tfrac{1}{2}\omega S[1+\sqrt{3}(1-2b)\mu_0] \times \exp[-(\tau_0-\tau)/\mu_0], \quad (22)$$

where I^+ and I^- are defined by the set of equations

$$\int_{-1}^{+1}\tilde{I}(\tau,\mu)\mu d\mu=(I^+-I^-)/\sqrt{3}, \quad (23)$$

$$\tilde{I}(\tau,\mu)=I(\tau,\mu)-S\delta[\mu-(-\mu_0)]\exp[-(\tau_0-\tau)/\mu_0]. \quad (24)$$

It is noted from (24) that $\tilde{I}(\tau,\mu)$ represents the diffuse component of radiation. Also, we see from (23) that I^+ denotes the intensity of radiation traveling in the $\mu=1/\sqrt{3}$ direction, and I^-, that of the radiation in the $\mu=-1/\sqrt{3}$ direction. The choice of $\mu=1/\sqrt{3}$, $-1/\sqrt{3}$ is based on the two-point Gaussian quadrature formula.

The backscattering factor b and the forward scattering factor f are defined by

$$2b=1=\frac{1}{2}\int_{-1}^{+1}p(\mu)\mu d\mu, \quad (25)$$

$$f=1-b. \quad (26)$$

Physically, b represents the fraction of energy scattered in the backward direction.

Assuming that the earth's surface reflects diffusely, the boundary conditions (19) and (20) can be expressed in terms of I^+ and I^- as

$$I^+(0)=r_s[I^-(0)+\sqrt{3}\mu_0 S\exp(-\tau_0/\mu_0)] \quad (27)$$

and

$$I^-(\tau_0)=I_d. \quad (28)$$

Even with the simplifications afforded by the two-stream approximation it is not possible to obtain closed-form analytic solutions of (27) and (28) for an inhomogeneous atmosphere. However, the equations can be numerically solved by dividing the model layer into a number of sublayers depending on the degree of accuracy required. The details of the procedure can be found elsewhere (Venkatram, 1977).

3. Results and discussion

a. Initial conditions and parameters used in simulations

The conservation equations were solved numerically using an implicit finite-difference scheme. The grid

TABLE 1. Summary of surface parameters and pollutant properties used in simulations.

Surface Parameters

$k_s=2.0\ \mathrm{W^{-1}\,m^{-1}\,^\circ C^{-1}}$	Latitude = 42.5°N
$\rho_s=1.5\times10^3\ \mathrm{kg\ m^{-3}}$	Solar declination = 11°N
$C_{ps}=1.0\times10^3\ \mathrm{J^{-1}\,kg^{-1}\,^\circ C^{-1}}$	$H=2000$ m
$r_s=0.2$	$\Delta=0.5$ m
$e_t=1.0$	Surface temperature = 285 K
$H=0.1$	$u_g=2.88\ \mathrm{m\ s^{-1}}$
$z_0=0.01$ m	$v_g=1.88\ \mathrm{m\ s^{-1}}$

Aerosol Properties

$\beta_{ex}=10^{-6}\ \mathrm{m^2\ \mu g^{-1}}$
$f=0.85$
$\omega=0.90$

Simulations

NP No radiative participation by gaseous pollutants (thermal) and aerosols (solar).
P Participation by gaseous pollutants and aerosols.
SP Participation by aerosols only.
TP Participation by gaseous pollutants only.

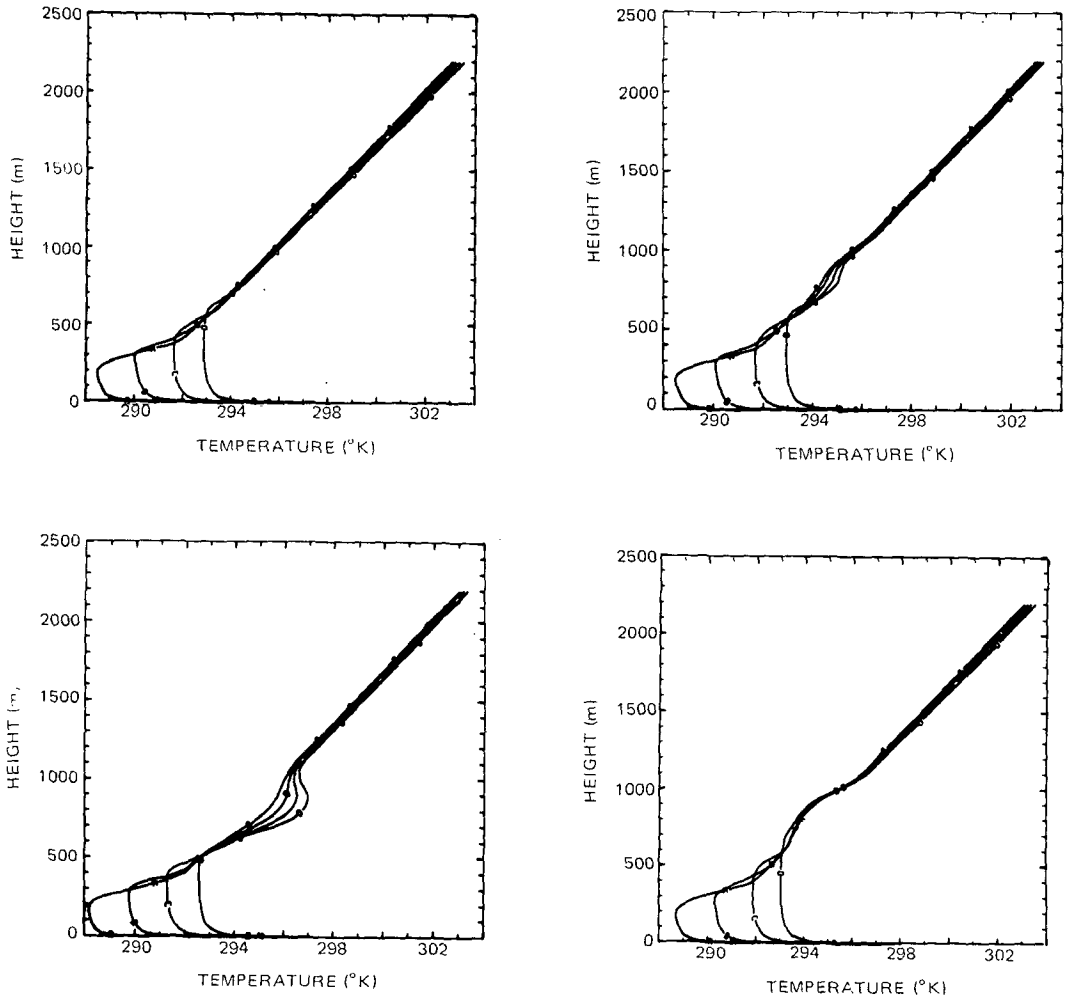

FIG. 9. As in Fig. 8 except for 0900–1200.

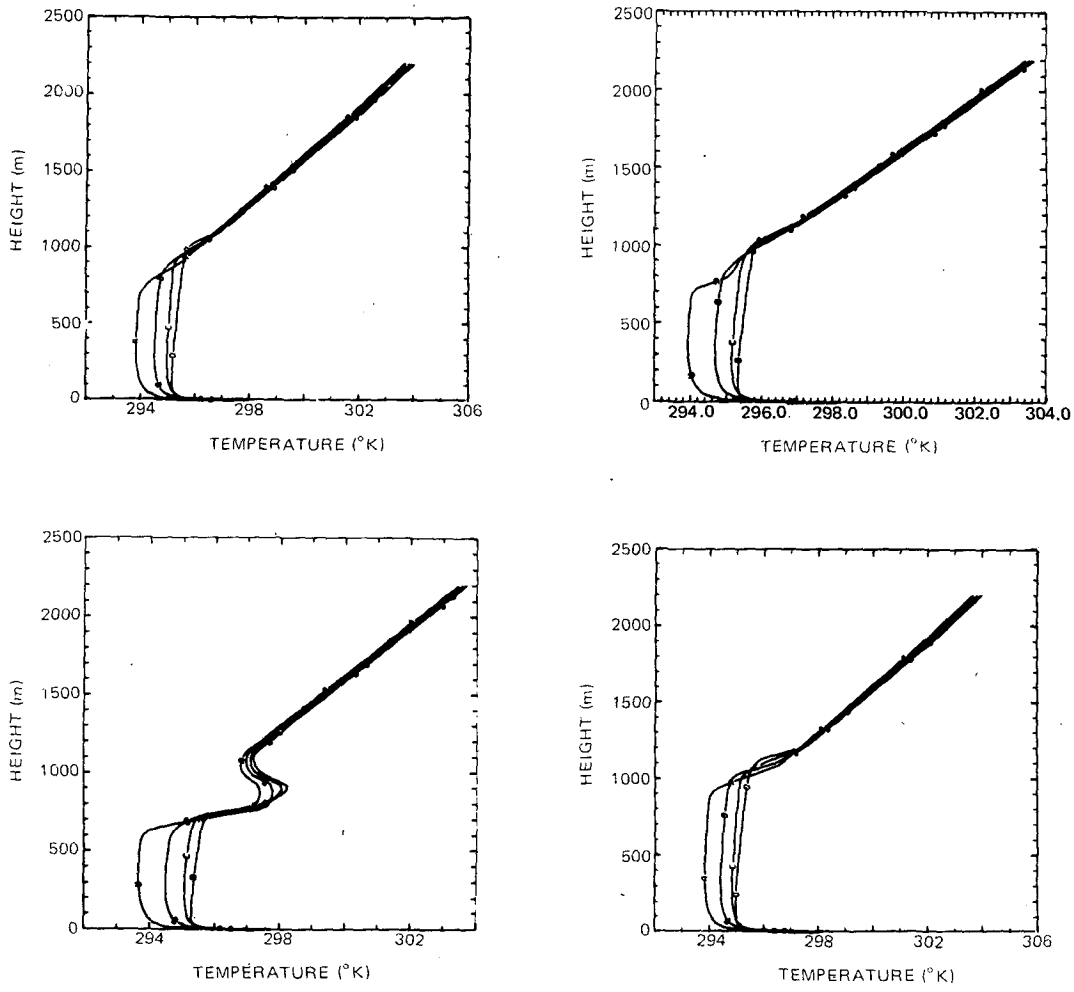

FIG. 10. As in Fig. 8 except for 1300–1600.

system was designed to provide better resolution near the air–soil interface. Table 1 presents the physical properties, parameters utilized in this study and the simulations performed.

The test simulation was started at 0500 local time, and the initial conditions were representative of early morning atmospheric conditions during the period August–September 1953 over the flat prairies at O'Neill, Nebr. Specifically, the potential temperature profile was based on Carson's (1973) comments. Carson has made a detailed study of the O'Neill profiles (Lettau and Davidson, 1957) and concludes that the typical early morning profile is characterized by two gradients. The nocturnally established surface inversion is typically about 400 m deep and has a gradient of about 18×10^{-3} K m^{-1}. The layer above it, extending to about 2 km, has a typical gradient of about 6×10^{-3} K m^{-1}. Thus, using this information, an initial potential temperature profile was constructed after assuming an appropriate surface temperature. The water vapor concentration was assumed to be uniform at 5 g m^{-3}. The soil temperature was taken to be uniform at the surface temperature over the depth of the soil layer. The upper atmospheric data (temperature and water vapor) were taken from McClatchey *et al.*, (1972).

The aerosol parameters are based on calculations by Hansen and Pollack (1970). The extinction coefficient was chosen so that with the average mass loadings obtained in the simulations the optical thickness in the solar spectrum would be in the range from 0.1 to 0.2. These values of optical thickness are based on measurements of Herman *et al.* (1971) which place the mean atmospheric optical thickness (0.55 μm) around 0.1. The single-scattering albedo of 0.9 corresponds to a slightly absorbing aerosol (Rasool and Schneider, 1971). Ammonia was used as a representative gaseous pollutant.

b. Sample simulations

1) BOTTOM OF POLLUTANT LAYER LOCATED AT 300 M

The first set of simulations was performed with the lower edge of the pollutant layer located at 300 m. The layer was taken to be 300 m thick and the maximum

concentration was assumed to be 400 μg m^{-3}. This relatively large value was chosen to highlight radiative effects. The results of four different simulations are shown in Figs. 1–3. These figures illustrate the evolution of the potential temperature profiles over a 12 h period. The temperature profiles of simulation NP (non-participating pollutants) show the usual development with the nocturnally established inversion being eroded away as the mixed layer grows during the day. The results of simulation TP show the cooling effect of pollutants which participate only in the thermal spectrum. The cooling is quite pronounced within 4 h, and the mixed layer grows rapidly as the stable layer above it is cooled. At the same time the thermal participation of the pollutants creates a slight inversion at the top of the pollutant layer. This inversion is not strong enough to slow down the growth of the mixed layer. The formation of this inversion has been predicted in theoretical studies by Atwater (1970) and Bergstrom and Viskanta (1973). Observations (Bornstein, 1968; Rouse *et al.*, 1973) of elevated inversions over industrial areas lend some validity to this result.

Simulation SP (aerosol participation only) shows the effects of aerosol heating. In about 8 h the heating leads to the formation of a highly stable layer at a height of around 400 m. The layer above the stable layer is marked by a negative potential temperature gradient. It is evident from Fig. 2 that the sharp temperature gradient caused by aerosol heating effectively impedes the growth of the mixed layer. It is only after 9 h that the mixed layer is able to penetrate the inversion, and the growth thereafter is relatively rapid as the layer above is unstable.

The results of simulation P (participation by aerosols and gases) show the opposing effects of gases and aerosols. The heating caused by aerosols is counteracted to a certain extent by the cooling induced by the gaseous pollutants. Fig. 2 shows the pollutant layer heating up at the bottom and cooling at the top. The stabilizing effect of heating prevents the mixed layer

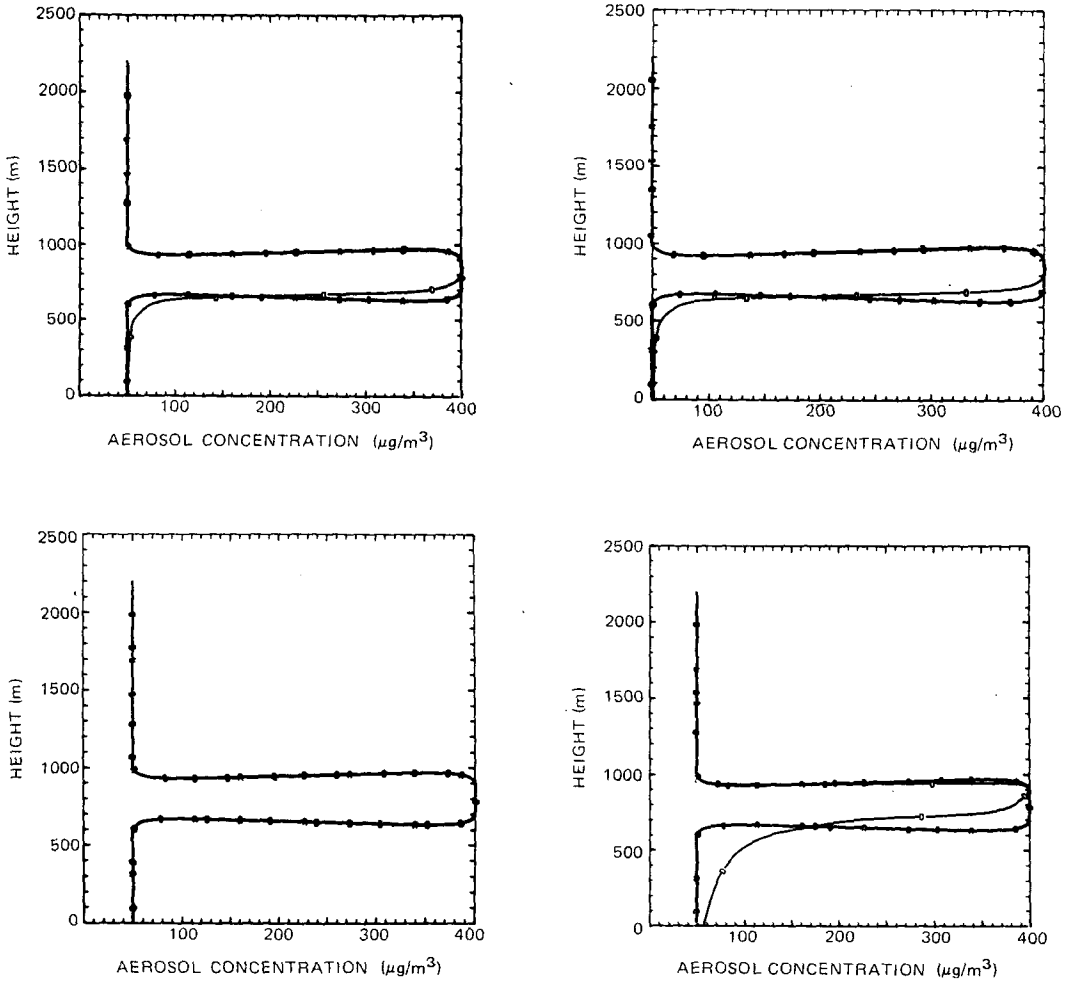

FIG. 11. Aerosol concentration profiles for 0900–1200 with elevated pollutant layer at 600 m. Otherwise as in Fig. 8.

from growing as rapidly as in the case when there is no pollutant participation. Once the mixed layer penetrates the inversion it grows at a rate comparable with that of simulation NP.

Figs. 4–6 show the effect of radiative participation of pollutants on pollutant dispersal. During the first 4 h, the pollutant layer is unaffected as the mixed layer has not yet grown high enough to disperse the pollutants. During the following 4 h, the effect of pollutants is evident from the different rates of pollutant dispersal as shown in Fig. 5. Thermal participation by increasing the initial rate of mixed-layer growth is conducive to pollutant dispersal, while solar participation decreases the rate at which pollutants diffuse away from the pollutant layer. At the end of 8 h after the beginning of the simulation, the surface pollutant concentration is 180 $\mu g\ m^{-3}$ for no participation, 170 $\mu g\ m^{-3}$ for thermal and solar participation, 135 $\mu g\ m^{-3}$ for solar participation only, and 200 $\mu g\ m^{-3}$ for thermal participation only. From Fig. 6, it can be seen that solar participation can slow down pollutant dispersal even after 9 h. Once the mixed layer penetrates the inversion created by solar heating, pollutants are mixed rapidly and radiative participation becomes unimportant.

Fig. 7 shows the effect of radiative participation on the growth of the mixed layer. It is seen that the largest mixed-layer heights (1400 m) occur for the simulations in which there is solar participation. An explanation for this apparent anomaly is fairly simple. Solar heating creates a sharp inversion at the height of the aerosol layer; at the same time the layer above the inversion is destabilized. Initially, the inversion created by solar heating inhibits the growth of the mixed layer, but once the mixed layer penetrates the inversion its growth is relatively more rapid than for the other simulations as the layer above the inversion is unstable. The effects of the destabilizing influence of solar heating are evident on the second day when the mixed-layer growth is greatest (1420 m) for the simulations with solar participation. Cooling induced by gaseous pollutants helps the growth of the mixed layer as evidenced by the larger mixed-layer heights for the simulations with thermal participation.

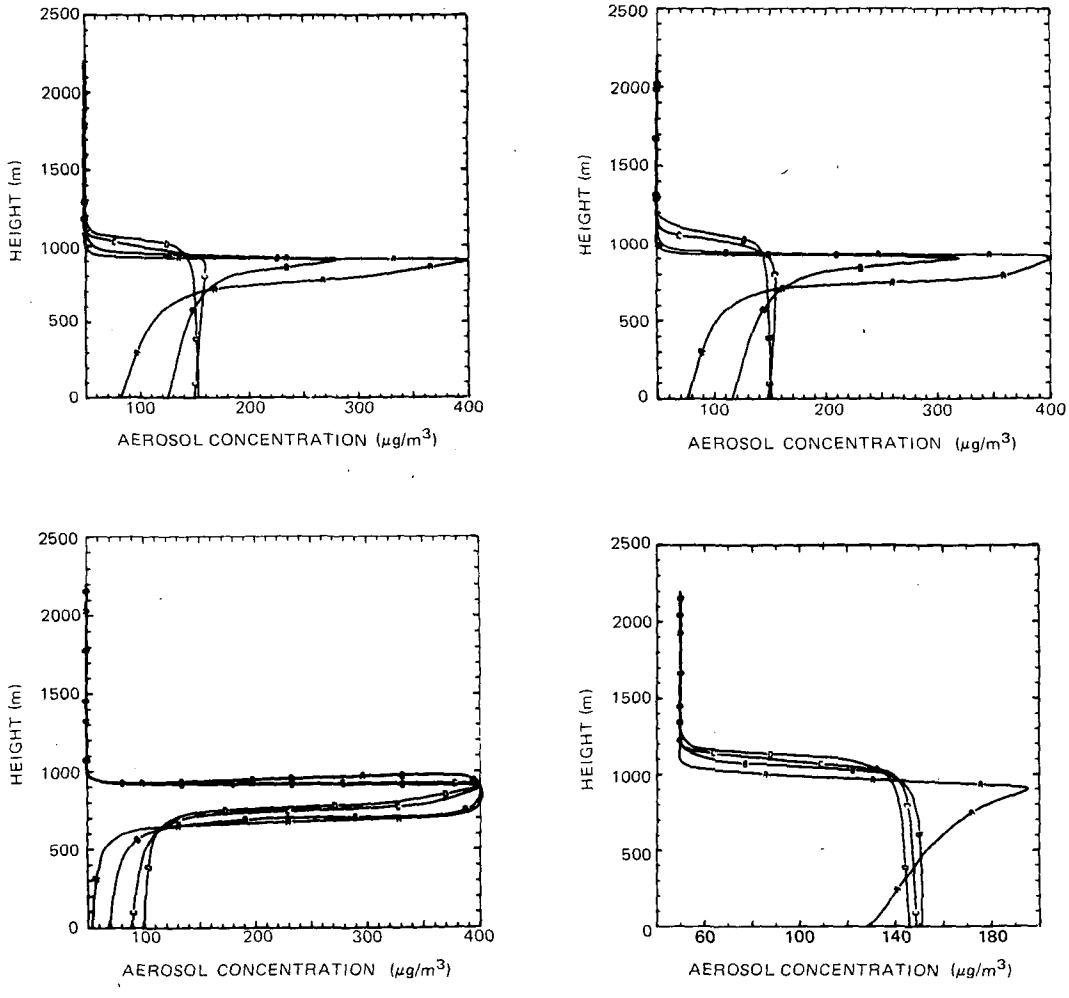

FIG. 12. As in Fig. 11 except for 1300–1600.

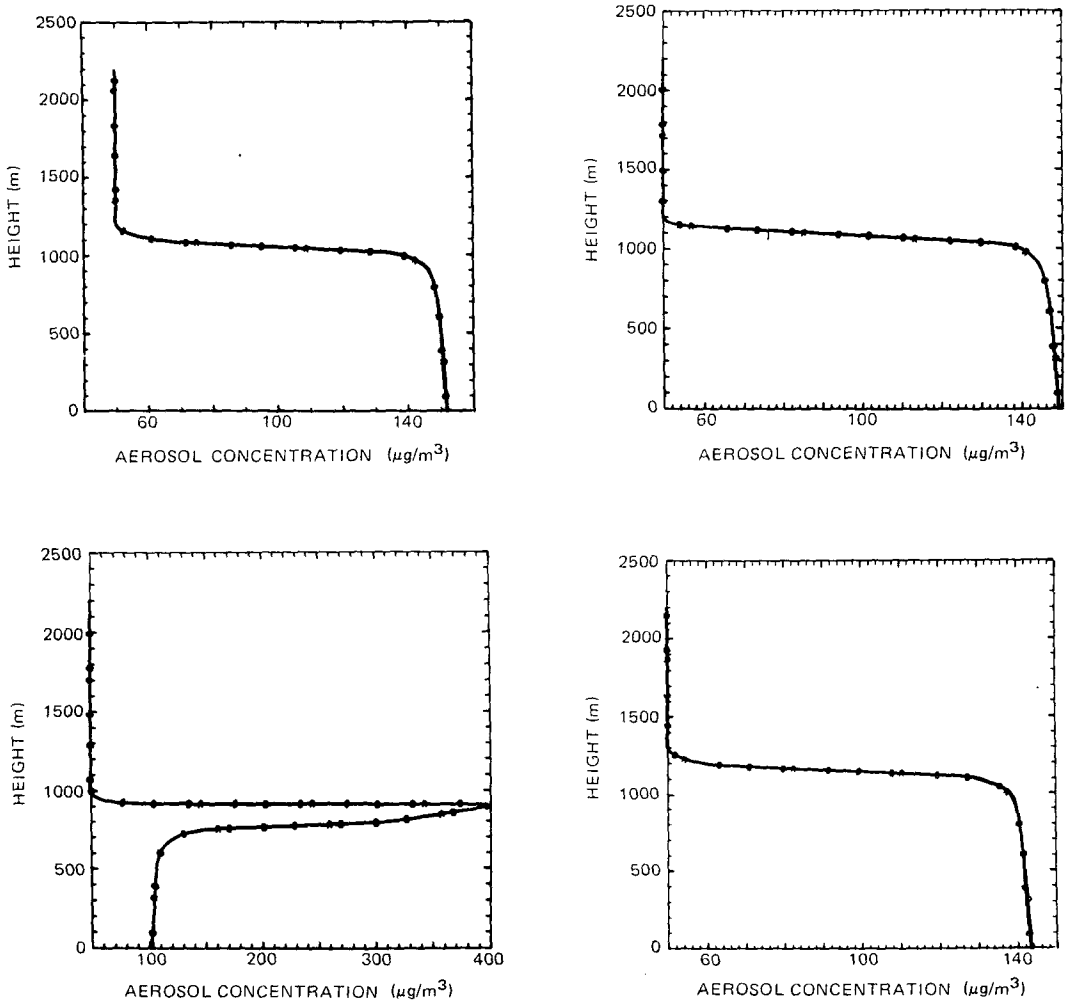

FIG. 13. As in Fig. 11 except for 1700 to 2000.

2) BOTTOM OF POLLUTANT LAYER LOCATED AT 600 M

A second set of simulations was performed to determine the effect of the height of elevated pollutant layer on thermal structure and pollutant dispersal. The lower edge of the pollutant layer was located at 600 m. Figs. 8–13 illustrate the variation of the temperature and concentration profiles. The results indicate the same trends as those of the first set of simulations. However, as the greater height of the pollutant layer allowed the pollutant-induced heating and cooling to proceed over a longer period of time, the inversions formed were considerably sharper as indicated in Fig. 10. It is seen from Fig. 10 that the inversion created by solar heating is large enough to prevent the growth of the mixed layer beyond the height of the pollutant layer. The effect of the creation of this "lid" on pollutant dispersal is evident in Figs. 12 and 13.

Table 2 shows the effect of radiative participation by pollutants on pollutant dispersal. It is seen that initially solar heating due to aerosols slows pollutant dispersal from the elevated layer as indicated by the lower surface concentrations for the simulations with solar participation. The concentrations of simulation P show that cooling induced by the gaseous pollutant helps the mixed layer penetrate the sharp inversion created by the solar heating due to aerosols. Once the mixed layer penetrates the inversion its growth is more rapid than for the other simulations because the region above the inversion is unstable. The more rapid growth and consequently the higher final mixed-layer thickness is indicated by the lowest value (125.7 μg m^{-3}) of surface concentration at 0300 of the second day. It is interesting to note that the greatest surface (1 m) aerosol concentration occurs for the simulation in which aerosols are the only participants. An explanation for this can be found by examining the effect of solar heating on the height of the mixed layer. Solar heating does inhibit dispersal as indicated by the lower surface pollutant concentrations until 1100 of the second day. At the same time the sharp inversion induced by solar energy absorption prevents the vertical expansion of the mixed layer. Thus, the pollutants which are allowed to disperse

TABLE 2. Comparison of aerosol concentrations ($\mu g\ m^{-3}$) at 1 m (elevated layer at 600 m).

Time	Aerosol concentrations NP	P	SP	TP
0700	50.0	50.0	50.0	50.0
0900	50.0	50.0	50.0	50.0
1100	50.0	50.0	50.0	50.0
1300	81.7	76.3	53.4	128.4
1500	149.7	147.7	87.7	149.0
1700	152.0	149.3	102.6	143.8
1800	151.7	149.0	102.7	143.3
2100	151.7	149.0	102.7	143.3
2300	151.7	149.0	102.7	143.3
0100	151.7	149.0	102.7	143.3
0300	141.7	149.0	102.7	143.3
0500	151.7	149.0	102.8	143.3
0700	151.7	149.0	102.8	143.3
0900	141.4	149.0	103.0	143.1
1100	140.8	147.9	104.1	142.2
1300	144.9	138.6	133.4	136.8
1500	134.4	129.3	133.6	129.9
1700	130.2	125.8	141.5	126.6
1900	130.1	125.7	141.5	136.4
2100	130.1	125.7	141.5	136.4
2300	130.1	125.7	141.5	136.4
0100	130.1	125.7	141.5	136.4
0300	130.1	125.7	141.6	136.4

over a smaller vertical extent reach higher concentrations at the surface.

Fig. 14 illustrates the effect of radiative participation on the growth of the mixed layer. It is evident that the height of the elevated pollutant layer determines the effect of solar heating in the PBL. When the pollutant layer is at 600 m solar heating proceeds over a longer period of time and the inversion formed is large enough to limit the growth of the mixed layer. The mixed layer is not able to penetrate the inversion and does not grow beyond 820 m. It can be seen that cooling induced by gaseous pollutants helps the mixed layer to grow. This effect is evident in the simulation in which there is thermal and solar participation. While the mixed layer is not able to penetrate the inversion when aerosols are the only radiative participants, it does so with the assistance of gaseous cooling. As the layer above the inversion is unstable the mixed layer grows to a height of 1420 m, the largest value for the simulations.

4. Conclusions

The results of the study show that elevated layers of pollutants can play a very important role in controlling mixed layer expansion. It is found that pollutant-induced cooling or heating modifies the stability of the inversion capping the mixed layer. Solar heating due to pollutants leads to the formation of sharp inversions which initially hinder the growth of the mixed layer. However, once the mixed layer penetrates the inversion its growth is relatively rapid as the formation of the localized stable layer is accompanied by the creation of an unstable layer above it. Thus, the effect of solar participation by pollutants greatly depends on whether the mixed layer is able to penetrate the solar-heating-induced inversion. When the elevated layer is located around 300 m, the inversion is eroded by the mixed layer. However, when the pollutant layer is located at

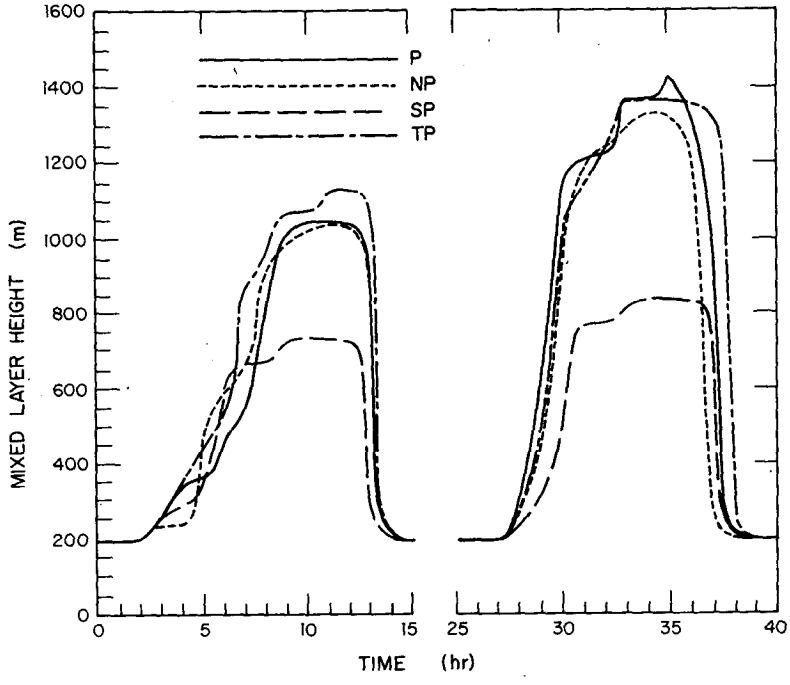

FIG. 14. Variation of mixed-layer height with time-elevated pollutant layer at 600 m.

600 m, solar heating in the absence of the turbulent diffusion proceeds over a longer period of time and the inversion formed is strong enough to prevent the mixed layer from growing beyond the elevation of the pollutant layer. Cooling due to thermal participation by pollutants generally helps the growth of the mixed layer.

By affecting mixed layer growth, radiative participation by pollutants also modifies pollutant dispersal from the elevated pollutant layer. These results have important implications from the point of air pollution meteorology (especially fumigation) in which it is generally assumed that pollutants are passive.

It is worthwhile to point out some of the shortcomings of this modeling effort. It is noted that the treatment of turbulence in the unstable layer above the pollutant-induced inversion is not satisfactory. It is probable that the negative potential temperature gradient gives rise to turbulence which might destroy the inversion more rapidly than our model predicts. Clearly, satisfactory modeling of such events requires an understanding of turbulence in isolated unstable layers. Specification of turbulent length scales in the unstable layers is a problem. Although we have not attacked this problem in this paper we believe that we have demonstrated the importance of radiatively active elevated pollutant layers.

Acknowledgments. This research was supported by the Meteorology and Assessment Division of the U. S. Environmental Protection Agency under Grants R801102 and R803514 to Purdue University. Computer facilities were provided by Purdue University and the National Center for Atmospheric Research which is sponsored by the National Science Foundation.

APPENDIX

List of Symbols

c_p	specific heat at constant pressure
F	total radiative flux in $+z$ direction
f	Coriolis parameter or forward scattering factor
g	acceleration due to gravity
K	turbulent eddy diffusivity
k	thermal conductivity, turbulent kinetic energy or von Kármán constant
M_{C_n}	surface pollutant source flux
p	pressure
S_{C_n}	volumetric pollutant source rate
T	thermodynamic temperature
t	time
u	horizontal velocity along x axis
v	horizontal velocity along y axis
z	vertical coordinate
z_0	roughness length
α	thermal diffusivity $[=k/\rho C_p]$
γ_c	countergradient heat flux parameter
θ	potential temperature
ρ	density

Subscripts

C	associated with eddy diffusivity for species
C_n	species
g	geostrophic
H	heat
M	momentum
0	surface value
s	solar or soil
wv	water vapor

REFERENCES

Atwater, M. A., 1970: Investigation of the radiation balance for polluted layers of the urban environment. Ph.D. thesis, New York University, 116 pp.

Bergstrom, R. W., and R. Viskanta, 1973: Modeling the effects of gaseous and particulate pollutants in the urban atmosphere. Part I: Thermal structure. *J. Appl. Meteor.*, **12**, 901–912.

Blackadar, A. K., 1962: The vertical distribution of wind and turbulent exchange in a neutral atmosphere. *J. Geophys. Res.*, **67**, 3095–3120.

Bornstein, R. D., 1968: Observations of the urban heat island effect in New York City. *J. Appl. Meteor.*, **7**, 575–582.

Businger, J. A., 1972: Turbulent transfer in the atmospheric surface layer. *Workshop in Micrometeorology*, D. A. Haugen, Ed., Amer. Meteor. Soc., 67–100.

Carson, D. J., 1973: The development of a dry inversion-capped convectively unstable boundary layer. *Quart. J. Roy. Meteor. Soc.*, **99**, 450–467.

Deardorff, J. W., 1974: Three-dimensional numerical study of the height and mean structure of a heated planetary boundary layer. *Bound.-Layer Meteor.*, **7**, 81–106.

——, 1967: Empirical dependence of the eddy coefficient for heat upon stability above the lowest 50 m. *J. Appl. Meteor.*, **6**, 631–643.

Delage, Y., 1974: A numerical study of the nocturnal atmospheric boundary layer. *Quart. J. Roy. Meteor. Soc.*, **90**, 136–146.

Donaldson, C. duP., 1973: Construction of a dynamic model of the production of atmospheric turbulence and the dispersal of atmospheric pollutants. *Workshop in Micrometeorology*, D. A. Haugen, Ed., Amer. Meteor. Soc., 313–390.

Estoque, M. A., 1963: A numerical model of the atmospheric boundary layer. *J. Geophys. Res.*, **68**, 1103–1113.

France, W. L., and D. Williams, 1966: Total absorptance of ammonia in the infrared. *J. Opt. Soc. Amer.*, **56**, 70–74.

Hansen, J. E., and J. B. Pollack, 1970: Near-infrared light scattering by terrestrial clouds. *J. Atmos. Sci.*, **27**, 265–281.

Halstead, M. R., R. Richman, W. Covey and J. Merrman, 1957: A preliminary report on the design of a computer for micrometeorology. *J. Meteor.*, **14**, 308–325.

Herman, B. M., S. R. Browning and R. J. Curran, 1971: The effect of atmospheric aerosols on scattered sunlight. *J. Atmos. Sci.*, **28**, 419–428.

Kalmykov, V. G., A. N. Sherstyuk and T. V. Shulgina, 1975: The mixing length in a wall boundary layer. *Fluid Mech. Sov. Res.*, **4**, 66–69.

Kondratyev, K. Ya., 1969: *Radiation in the Atmosphere.* Academic Press, 912 pp.

——, O. B. Grishechkin Vassilyev and L. S. Ivlev, 1974: Spectral radiative flux divergence and its variability in the troposphere in the 0.4–2.4 μm region. *Appl. Opt.*, **13**, 478–486.

Kuhn, P. M., 1963: Radiometersonde observations of infrared flux emissivity of water vapor. *J. Appl. Meteor.*, **2**, 368–378.

Launder, B. E., and D. B. Spalding, 1972: *Lectures in Mathematical Models of Turbulence.* Academic Press, 169 pp.

Lettau, H. H., and B. Davidson, 1957: *Exploring the Atmosphere's First Mile.* Vol. 2. Pergamon Press, 201 pp.

Ludwig, C. B., R. Bartle and M. Griggs, 1969: Study of air pollutant detection by remote sensors. NASA Contractor Rep. No. CR-1380, General Dynamics Corporation, San Diego, Calif.

Lusis, M. A., and H. A. Wiebe, 1976: The rate of oxidation of sulphur dioxide in the plume of a nickel smelter stack. *Atmos. Environ.*, **10**, 793–798.

Lykosov, V. N., 1972: Unsteady state in the planetary boundary layer of the atmosphere. *Izv. Atmos. Ocean Phys.*, **8**, 85–91.

McClatchey, R. A., R. W. Fenn, J. E. A. Selby, F. E. Volz and J. S. Garing, 1972: Optical properties of the atmosphere, 3rd. Ed. AFCRL-72-0497, Environ. Res. Pap. No. 411, 108 pp.

Peterson, J. T., 1969: The climate of cities: A survey of recent literature. NAPCA Publ. No. AP-59, 48 pp.

Rasool, S. I. and S. H. Schneider, 1971: Atmospheric carbon dioxide and aerosols: Effects of large increases on global climate. *Science*, **173**, 138–141.

Rouse, W. R., D. Noad and J. McCutcheon, 1973: Radiation, temperature and atmospheric emissivities in a polluted urban atmosphere at Hamilton, Ontario. *J. Appl. Meteor.*, **12**, 798–807.

Sasamori, T., 1970: A numerical study of atmospheric and soil boundary layers. *J. Atmos. Sci.*, **27**, 1122–1137.

Sagan, C., and J. B. Pollack, 1967: Anisotropic non-conservative scattering and the clouds of Venus. *J. Geophys. Res.*, **72**, 469–477.

Sherstyuk, A. N., 1969: Reports at Scientific and Technical Conference on the Current Results of Research and Design Work for 1968–1969. MEI Press, Moscow.

Shekter, F. N., 1950: Calculation of thermal radiative fluxes in the atmosphere. *Tr. Gl. Geofiz. Observ.*, No. 22, 84–86.

Shir, C. C., and R. D. Bornstein, 1977: Eddy exchange coefficients in numerical models of the planetary boundary layer. *Bound.-Layer Meteor.*, **11**, 171–185.

Taylor, P. A. 1974: Urban meteorological modeling—Some relevant studies. *Advances in Geophysics*, Vol. 18B, F. N. Frankiel and R. E. Munn, Eds., Academic Press, 173–185.

Telford, J. W., and J. Warner, 1964: Fluxes of heat and vapor in the lower atmosphere derived from aircraft observations. *J. Atmos. Sci.*, **21**, 539–548.

Tennekes, H., 1974: The atmospheric boundary layer. *Phys. Today*, **17**, 52–63.

——, and J. L. Lumley, 1972: *A First Course in Turbulence.* The MIT Press, 300 pp.

Tien, C. L., 1973: Band and total emissivity of ammonia. *Int. J. Heat Mass Transf.*, **16**, 856–857.

Venkatram, A., 1977: Effects of aerosol induced heating on the convective boundary layer. ARQL Rep. 4/77. [Available from AES, Downsview, Ontario, Canada.]

——, and R. Viskanta, 1976: Radiative effects of pollutants on the planetary boundary layer. EPA Rep. EPA-60014-76-039.

Wang, W., and G. A. Domoto, 1974: The radiative effect of aerosols in the earth's atmosphere. *J. Appl. Meteor.*, **13**, 521–534.

Wyngaard, J. C., O. R. Cote and K. S. Rao, 1974: Modeling the atmospheric boundary layer. *Advances in Geophysics*, Vol. 18A, F. N. Frankiel and R. E. Munn, Eds., Academic Press, 193–211.

Yamada, T., and G. Mellor, 1975: A simulation of the Wangara atmospheric boundary layer data. *J. Atmos. Sci.*, **32**, 2309–2329.

Zdunkowski, W. G., R. W. Welch and J. Paegle, 1976: One-dimensional numerical simulation of the effects of air pollution on the planetary boundary layer. *J. Atmos. Sci.*, **33**, 2399–2414.